PAST SHIFTS IN THE GENERAL CIRCULATION:

CAUSATION, STRUCTURE, AND EFFECTS

ON HYDROCLIMATE

by

Jonathan James Rutz

A thesis submitted to the faculty of
The University of Utah
in partial fulfillment of the requirements for the degree of

Master of Science

Department of Atmospheric Sciences

The University of Utah

May 2011

The University of Utah Graduate School

STATEMENT OF THESIS APPROVAL

The thesis of **Jonathan James Rutz**

has been approved by the following supervisory committee members:

Thomas Reichler	, Chair	**11/16/2010**
		Date Approved
John Horel	, Member	**11/16/2010**
		Date Approved
Courtenay Strong	, Member	**11/16/2010**
		Date Approved

and by **James Steenburgh** , Chair of

the Department of **Atmospheric Sciences**

and by Charles A. Wight, Dean of The Graduate School.

ABSTRACT

There is now abundant evidence that an important consequence of recent climate change is the displacement of key elements within the global circulation. Considerable uncertainty exists with regard to the sign and magnitude of these changes, and it is also not fully understood how the roles of individual anthropogenic forcings contribute toward their cause. Because of the potential impacts they may impose upon hydroclimate, these changes in the circulation, and particularly their causation, are of high interest. Our primary goal is to differentiate between the various anthropogenic forcings driving these shifts.

We analyze the results from long time-slice simulations performed using a state-of-the-art atmospheric general circulation model, which show that important features in the general circulation have shifted poleward since the preindustrial era. Many of these shifts are characterized by pronounced seasonality and exhibit a tendency to be maximized during the summer months of each respective hemisphere. Furthermore, the magnitude of these shifts tends to exhibit a greater variability both over the southern hemisphere and within the extratropical regions. While reductions in ozone and increases of greenhouse gas concentrations have played a role in causation, the indirect effects from feedback mechanisms have been dominant. In most cases, a linear addition of the changes produced in those experiments prescribed with individual forcings is nearly identical to that for an experiment performed with all forcings included. This result is

remarkably consistent, indicating that effects of the mechanisms that lead to changes in the circulation are approximately linearly additive.

TABLE OF CONTENTS

LIST OF FIGURES

ACKNOWLEDGEMENTS

First and foremost, I would like to thank my graduate advisor, Thomas Reichler, for the commitments of time and effort he has made towards guiding my research. I am also grateful to my committee members, professors John Horel and Court Strong, for their willingness to serve in this capacity. I also wish to extend appreciation to Junsu Kim and Paul Staten, both within the Climate Research Group at the University of Utah. Their assistance in making themselves both available to discuss the relevant topics and to aid in some of the technical aspects of my work has been instrumental to my progress. Finally, I would like to acknowledge my parents, James and Susanne Rutz, whose constant support and high expectations have provided the foundation not only for this work, but for anything I have accomplished.

CHAPTER 1

INTRODUCTION

Previous model-based studies have found that prominent features within the global atmospheric circulation have undergone important shifts in recent decades and that this process is likely to continue in the future. However, from an observational perspective, it is difficult to verify the nature and magnitude of the relevant trends due to the limited amount of data. Displacements of circulation features are of particular concern because they can induce shifts in water distribution and availability. This can potentially lead to negative impacts on society (Battisti and Naylor 2009) and ecosystems – strains that will likely be increased through continued population growth and climate change throughout the 21st century. Therefore, a thorough understanding of how the general circulation responds to anthropogenic activity is required.

Methodically investigating changes in the circulation is made difficult due to the complexity of the system, but nevertheless many studies have been carried out over the last decade. Initially, much of this work centered on changes in the annular modes, motivated by the seminal work of Baldwin and Dunkerton (2001) suggesting stratospheric influences on large-scale tropospheric weather patterns. This prompted intense investigation of how the high-latitude stratosphere was being altered, with the southern hemisphere (SH) receiving a majority of attention due to the well-documented

ozone hole. Gillett and Thompson (2003) used simulations from a climate model with prescribed ozone losses to reproduce the observed increase in circumpolar westerlies over the SH. The propagation of this feature to the surface as well as its seasonality was also accurately reproduced. Additionally, Son et al. (2009a) showed that the entire SH circulation was significantly impacted by changes in ozone concentrations.

In an early study, Kushner et al. (2001) showed that increases in anthropogenic greenhouse gases (GHGs) also played a role in altering the SH circulation. They described southward displacements of the SH jet and eddy momentum flux convergence among other features, which were seen in simulations using a version of the Geophysical Fluid Dynamics Laboratory (GFDL) climate model. Arblaster and Meehl (2006) found that while both ozone losses and GHGs play a role in modifying the SH stratospheric vortex, ozone losses were more important. More recently, Son et al. (2008) used an ensemble of stratosphere-resolving models to show that under a situation in which ozone recovery is realized, the observed increases in SH winds will likely be reversed, a scenario not accounted for in the simulations for Fourth Assessment Report of the Intergovernmental Panel on Climate Change (IPCC/AR4) . Results from Perlwitz et al. (2008) were in agreement with both of the previous two results.

Gillett et al. (2005) showed that an observed decrease in December – February (DJF) sea-level pressure (SLP) over the SH high latitudes could be accurately reproduced by a suite of climate models forced with ozone decreases, and that this led to an intensification of the westerlies. It was later indicated (Gillett et al. 2006) that these changes corresponded to an increase in the southern annular mode (SAM), Antarctic

cooling, and a poleward shift of the SH mean storm track. These results were then shown (Gillett and Stott 2009) to be applicable for all seasons.

The circulation over the northern hemisphere (NH) has also been vigorously studied. In particular, the northern annular mode (NAM), or Arctic Oscillation (AO), has been the focus of recent work. Gillett et al. (2003) found that modeling scenarios performed with anthropogenic forcings were not accounting for the observed magnitude of the northern hemisphere SLP changes that are consistent with an increase of the NAM. Miller et al. (2006) then used the IPCC/AR4 climate models to confirm that GHG increases cause a positive trend in the NAM, as well as the SAM. They also found the multi-model mean from this suite of models to be of the correct sign in annular mode (AM) changes, although weaker in magnitude – similar to the previous modeling work.

Further studies investigating the linkages between large-scale global warming and increases in the AO have also been undertaken. Moritz et al. (2002) pointed out that the large-scale warming continued to be occur even as a downward trend in the NAM was observed, indicating that interconnectedness between them was weak. Later, Cohen and Barlow (2005) generally supported this idea, implying that largescale warming and the sign of the AMs were largely unrelated. Using an ensemble of climate models, Kuzmina et al. (2005) showed that the NAM index rises with increases in CO_2 concentrations. It has been suggested (Overland and Wang 2005), however, that trends in the NAM may be more strongly related to internal variability than had previously been considered.

Changes in the Hadley Cell have also been the subject of recent studies. Mitas and Clement (2005) found evidence for an intensification of this feature in a variety of observational data. Using a global circulation model (GCM), discrepancies were found

between the model-derived changes and those seen in the observations (Mitas and Clement 2006). Lu et al. (2007) were able to show that the IPCC/AR4 models produced a poleward expansion of the Hadley circulation and an expansion of the associated subtropical dry zones. In a study relating model simulations to observations (Johanson and Fu 2009), the widening of the total Hadley circulation in both hemispheres since 1979 was found to be 2-5° latitude – a magnitude that could not be accounted for by internal variability. Hu and Fu (2007) used outgoing longwave radiation (OLR) as a proxy and found similar results, a total expansion of 2-4.5° latitude. Later observation-based work by Hu and Zhou (2010) found that this total widening varied by measure and ranged from 1.2° (SLP datasets) to 3.6° (OLR and precipitation datasets) for annual averages.

Potential changes in the structure of the tropopause were studied by Santer et al. (2003a). Reanalysis datasets were found to show a rise in tropopause height – a result confirmed by model simulations. Building upon these results, Santer et al. (2003b) showed that since 1979 the tropopause height has increased by several hundred meters. Furthermore, it was found that the effects of ozone and GHGs could account for 80% of this change. Using the Canadian Middle Atmosphere Model (CMAM), Fomichev et al. (2007) also found a rise in tropopause height due to the thermal expansion associated with a warmer troposphere. Son et al. (2009b) made the case that the tropopause could be affected by changes in ozone concentration.

Various studies have used changes in tropopause structure to examine changes in tropical width. For example, Seidel and Randel (2007) examined the behavior of the subtropical tropopause using radiosonde and reanalysis data. Using the frequency of high

tropopause (> 15 km) occurrences as a proxy, they arrived at results indicating a 5-8° latitude expansion of the tropical belt between 1979 and 2005, implying that models could not accurately account for the rate of this widening. Along with observational studies, model-based evidence for this expansion also exists (Reichler 2009). Recently, Lu et al. (2009) showed that changes in tropical width seen in the ERA40 reanalysis can be accurately simulated using an atmospheric GCM (AGCM) forced only by direct radiative forcings from natural and anthropogenic sources. In addition, it was found that tropical width decreased when the model was forced by observed SSTs alone. Other methods of measuring tropical width, not described here, have also been undertaken (Reichler 2009). Considering both model-based and observational studies, methods of assessing tropical expansion have arrived at values ranging from 1° to 8° latitude (Seidel et al. 2008). Such a range leaves a large amount of uncertainty regarding the actual nature and magnitude of these shifts. This uncertainty is, of course, not completely surprising given the short observational record in combination with the large amount of internal climate variability, and the fact that many important variables of climate interest, such as meridional wind and precipitation, are poorly observed.

An interesting aspect of recent work has been analysis of shifts in the hemispheric jets and the collocated storm tracks. Using the IPCC/AR4 climate models, Yin (2005) found a poleward shift in surface winds, storm tracks, precipitation, and increases in the index of the AMs. Using the ECHAM5 coupled climate, Bengtsson et al. (2006) also showed a poleward shift in storm track over the SH, which appears to be a response to shifts in SST gradients. Looking at reanalysis datasets, Archer and Caldeira (2008) found not only a poleward shift in jet location, but also an increase in jet altitude. Considering

the three-dimensional structure of the jet, Strong and Davis (2008) showed that jet location was strongly linked to the sign and magnitude of the NAM. Based on the IPCC/AR4 climate models, Lorenz and DeWeaver (2007) suggested that a rise in tropopause height was primarily responsible for shifts in the zonal jets as well as many above the above circulation features.

Changes in the location of the storm track have been shown to produce congruent shifts in hydroclimate (Lu et al. 2007). Investigating the linkages between the AMs and tropical expansion, Previdi and Liepert (2007) raised concern regarding dynamical impacts on the future hydrological cycle. Studies using various climate models by Bengtsson et al. (2006) and Gastineau et al. (2009) confirmed that significant increases in precipitation were being seen in model simulations, with much of the increase being associated with the extratropical cyclone tracks. Bengtsson et al. (2009) found these increases to be highly sensitive to the spatial pattern of SSTs, aligning well with earlier work by the same authors. Seager et al. (2007) showed that the southwestern United States would likely see a period of increased aridity due to changes in the circulation – a result that likely carries implications for other regions as well.

There has been debate as to which forcings are primarily responsible for inducing these changes in the circulation. Referencing earlier studies, especially with respect to the SAM, Karoly (2003) commented on the importance of understanding their individual contributions. Chen et al. (2007) stated that GHG increases and the indirect responses of the system would be the most important drivers of circulation change over the next century. Deser and Phillips (2009) showed that the influences of GHGs and indirect effects were nearly additive using the CAM3. Furthermore, they found that the roles of

direct and indirect effects in influencing the circulation are approximately equal. Karpechko et al. (2008) made the point that only ozone depletion leads to the previously mentioned downward propagation of stratospheric anomalies, while GHG primarily affects only the troposphere.

Despite these previous studies, there is still a large amount of uncertainty evident in the literature regarding the role of individual forcings in driving particular aspects of circulation change. In addition, only a select number of the above studies attempted to resolve the seasonality of the trends associated with these circulation changes. For these reasons, there are gaps in knowledge concerning both the causation and annual cycle of these shifts.

In this study, we use a model-based approach in an attempt to fill in the gaps mentioned above. First, we seek to resolve the uncertainty that exists regarding the sign and magnitude of trends in the general circulation since the pre-industrial era. Secondly, we explore indicators which have not been previously examined as a means to gain a more comprehensive understanding of these trends. Thirdly, we aim to fill the relative void in research related to both the influences of individual forcings and the annual cycle of changes associated with specific circulation features. Finally, we look to identify connections between these changes and the shifts they impose on hydroclimate. This is facilitated by running long time-slice simulations with a state-of-the-art AGCM, which is driven by different anthropogenic forcings and SSTs. These simulations enable us to fulfill our primary goal of understanding the contributions of the individual forcings to overall change.

In Chapter 2, we discuss the sources of our data and the methods employed to analyze it. Our results in Chapter 3 present our findings for changes in basic atmospheric quantities and selected circulation features. Chapter 4 provides a summary and discussion of our work.

CHAPTER 2

DATA AND METHODS

We make use of the GFDL model AM2 to perform long time-slice simulations that are driven by different combinations of anthropogenic forcings and SSTs. The AM2 has a grid point resolution of 2° latitude by 2.5° longitude and uses a finite-volume dynamical core to solve the equations of motion (Lin 2004). This model has both up to date physical parameterizations and a realistic climatological mean circulation (Reichler and Kim 2008).

In this study, we define averages over the period 1861-1870 as representative of the preindustrial era and 1997-2006 as representative of the present-day climate. The control run is forced using preindustrial conditions, with GHGs as well as seasonally varying zonal-mean ozone and lower boundary conditions set to their unperturbed mean values from the preindustrial era. CFCs are nonexistent. For ozone, 1979 concentrations are used as the control values. The preindustrial SSTs and sea-ice conditions (hereafter, simply SSTs) are derived from a preindustrial control simulation with the coupled companion model (GFDL CM2.1) of AM2, ensuring that the lower boundary conditions are realistic for this time period.

In addition to the control, we conduct a total of four different perturbed experiments, one of which is the control run described above. An overview of the

forcings prescribed for each perturbed experiment is provided in Table 1. Based upon their importance in driving large-scale climate change, we have chosen to further investigate the effects of ozone depletion and increases in GHGs on the circulation. Aerosol is not included in this study, but an experiment designed to assess its role is planned in future work. In addition, naturally occurring forcings (e.g., the solar cycle, volcanic events) are not considered. The control run consists of over 1000 years of simulation data and each of our experiments contains at least 500 years.

For the O3 experiment, the zonal-mean, seasonally varying ozone reflects its present-day distribution (Randel et al. 2002) while all other forcings are unchanged from the control run. The left panel in Figure 1 shows the changes in ozone concentration the O3 experiment is forced with. One can see that prescribed ozone losses are greatest at high latitudes and during the spring season, with the ozone hole being readily visible over the SH.

In the CO2 experiment, as shown in Table 1, present-day, well-mixed GHG concentrations are prescribed to the model, while ozone and boundary conditions are unchanged from the control run. We also perform an experiment in which the values of anthropogenic forcings are held fixed at preindustrial levels, but boundary conditions are representative of their present-day values. One can clearly see that the largest prescribed increases in SSTs with respect to the preindustrial era occur during winter at high latitudes (Figure 1, right panel). By keeping ozone and GHGs unperturbed during this simulation, we are able to isolate the response of the system that is not due to direct radiative forcing.

Finally, the ALL experiment is run with all three forcing components (ozone,

Table 1 Forcings for each experiment. Check marks indicate a perturbation with respect to the pre-industrial era using present-day values. Those for ozone and SST are shown in Figure 1. Perturbed (unperturbed) GHG concentrations are: CO_2 – 380 (280) ppm; CH_4 – 1754 (805) ppb, N_2O – 316 (275) ppb, CFC-11 – 260 (0) ppt, CFC-12 – 543 (0) ppt, CFC-113 – 82 (0) ppt, and CFC-22 – 144 (0) ppt.

	Ozone	GHG	SSTs
Control			
O3	✓		
CO2		✓	
SST			✓
ALL	✓	✓	✓

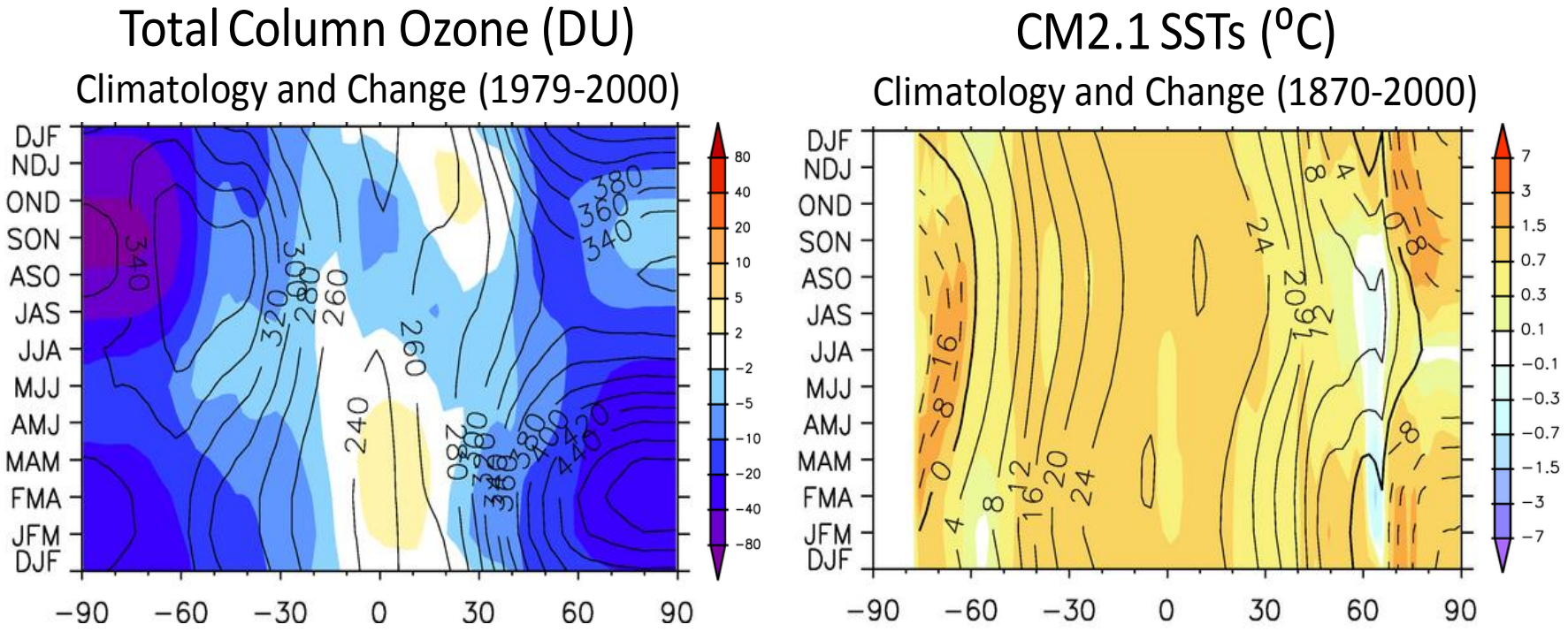

Fig. 1 Prescribed experiment forcings. Climatology (black lines) of ozone concentrations and SSTs from the control run and changes (shading) for the O3 experiment (left) and the SST experiment (right).

GHG, and SST) set to their present-day values.

In addition, this study utilizes the ERA40 reanalysis (referred to as ERA) from the European Centre for Medium-Range Weather Forecasts (Uppala et al. 2005) to supplement the model-produced data. We only examine reanalysis from 1979 or later, as it has been suggested that significant inconsistencies exist in data from the presatellite era (Randel et al. 2000).

In our analysis, we analyze climatological means taken over the entire simulation period available for each experiment. Changes or shifts are defined as the difference between the experiment climatology and that from the control run. For ERA, they represent linear trends from 1979-2001, multiplied by the number of years during this period. We focus on zonal-mean data unless otherwise stated. This affords us certain advantages: we aim for a diagnostic discussion of changes in the global circulation, and this allows for some simplicity in not having to contend with regional-scale issues. Linear interpolation is used to increase the native meridional resolution of our data to 0.1° latitude. The resulting meridional profiles are then smoothed using a Gaussian smoother with a ±15° latitude wide window.

For our examination of the tropopause height, we use the standard World Meteorological Organization definition – a lapse rate of 2 K/km or less, and obtain it following Reichler et al. (2003). To describe the structure of the tropopause, we employ a methodology invoked by Seidel et al. (2007) by dividing the atmosphere between 350 and 50 hPa into 60 vertical bins, each representative of a 5-hPa slab of atmosphere. We then count the number of tropopause occurrences found in a particular bin at all latitudes for each season, yielding a probability distribution function of tropopause pressure. This

offers a useful way to visualize the changes in the tropopause that have occurred in recent decades (Seidel et al. 2007, Seidel et al. 2008, Hu and Fu 2007, Lu et al. 2009). For the portion of our study which quantifies the seasonality of changes in tropopause structure, we adopt a different approach. We first derive a latitudinal profile of climatological mean tropical tropopause pressure (between ±20° latitude) for each experiment and the control. We then investigate shifts between the experiments and the control run in the latitudinal position of tropopause occurrences at a pressure 25 hPa below the tropical tropopause pressure.

The AMs (both SAM and NAM) are important measures of the atmospheric circulation over their respective hemispheres. In calculating the AMs, we follow the methodology suggested by Baldwin and Thompson (2009), using zonal-mean data. This approach was shown to provide an accurate assessment of the AMs while being readily employed for various model outputs (e.g., zonal-mean data only). We perform our analysis of the AMs with seasonal (3-month) mean SLP data, using the covariance matrix, as is standard. We also begin with yearly data, as opposed to decadal means for all other measures. An empirical orthogonal function (EOF) analysis is performed on our control run data using a routine provided in the Interactive Data Language. This operation yields a 'reference' EOF, on which we project the data from our experiments to understand how the leading modes over each hemisphere respond to the imposed forcings. We multiply the resultant changes in indices by a factor of $\sqrt{3}$ to account for the reduction in variability that arises from using seasonal mean data. The resulting indices can therefore be more directly compared against results from similar studies using monthly mean input data.

The statistical significance of our diagnosed changes is determined using a two-sided T-test on our data (Wilks 2006). Below is the relevant equation:

$$z = \frac{\overline{x_E} - \overline{x_C}}{\left[\left(\frac{1}{n_E} + \frac{1}{n_C}\right)\left\{\frac{(n_E - 1)\tilde{s}_E^2 + (n_C - 1)\tilde{s}_C^2}{n_E + n_C - 2}\right\}\right]^{1/2}} \quad ,$$

where x_i represents the data, n_i represents the number of years or decades for a given experiment, s_i^2 denotes the variance, and the subscripts, E or C, denote either a selected experiment or the control run, respectively. The quantity z follows the t-distribution with $\upsilon = n_E + n_C - 2$, where υ is the number of degrees of freedom. For changes to be significant, the value for z must be greater than the critical value of the t-distribution at a given significance level, α, for which we always choose 95%. In determining the statistical significance of the linear trends derived from the ERA40 reanalysis, we follow the methodology of Santer et al. (2000). The degrees of freedom are essentially determined by the number of years or decades in the control run (over 1000 years) and the experiment (over 500 years), or the number of years in the reanalysis.

CHAPTER 3

RESULTS

We now present the results of our analysis, which we divide into three sections: change in basic atmospheric quantities (3.1) and change in selected circulation indicators – both dynamical (3.2) and hydrological (3.3). The section on change in basic quantities examines fields which provide a broad overview of the general circulation. In the section on change in selected circulation indicators, we examine the forcings responsible for shifts in circulation features, as well as their seasonality.

3.1 Change in Basic Atmospheric Quantities

Figure 2 displays zonal-mean cross-sections of change in a number of key atmospheric features throughout the troposphere and lower stratosphere. Each column includes results from our four experiments as well as those seen in ERA (bottom). The shading shows changes in mean climate for each of our experiments with respect to the control run. For ERA, shading represents linear trends from 1979-2001. This season shown, DJF, was chosen because it coincides with Austral summer, a season in which shifts in many circulation indicators are most pronounced, particularly over the SH.

The first column in Figure 2 shows how the thermal structure of the atmosphere changes in response to the various forcings. In O3, the model develops significant

Fig. 2 Change in basic atmospheric quantities during DJF. Results are presented (from left to right) for T (K), U (m/s), Ψ (10^9 kg/s), $-\partial/\partial y$(u'v') (10^{-6} m^2/s^2), and the tropopause PDF (days/season). Thin black lines show climatological contours derived from the control run, which for Ψ and $-\partial/\partial y$(u'v') are one order of magnitude larger than those of their respective color scales. The black line shown in the last column denotes the climatological mean tropopause location (from the control run for the experiments; from 1979-2001 for the observations). Shading shows changes from both model-derived and observational data, where the linear trend from 1979-2001 is shown for the latter. Hatching shows changes which are non-significant according to a two-sided T-test at the 95% confidence interval. Units on the Y-axis are atmospheric pressure in hPa.

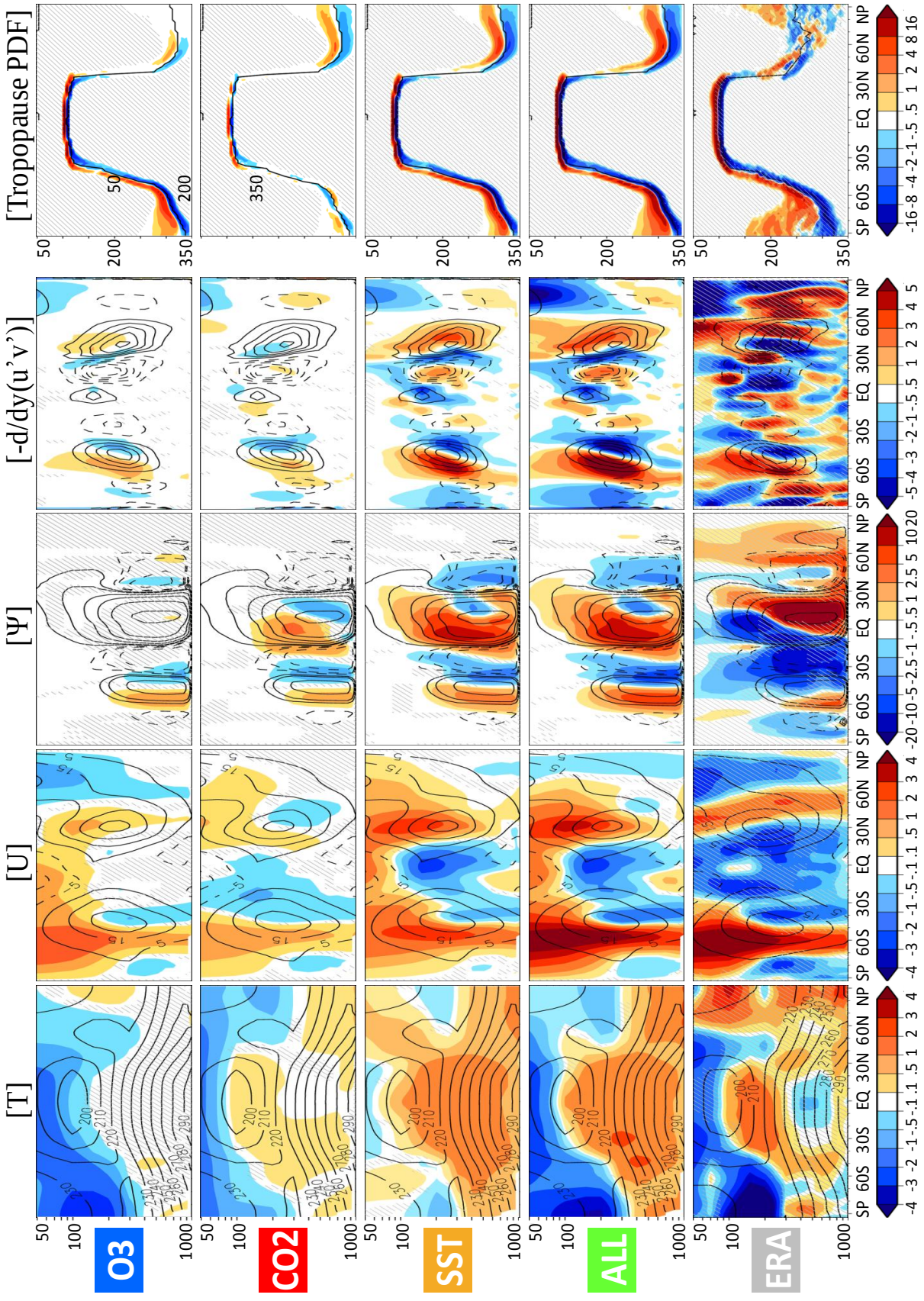
[T]
[U]
[Ψ]
[-d/dy(u'v')]
[Tropopause PDF]
O3
CO2
SST
ALL
ERA
SP 60S 30S EQ 30N 60N NP

stratospheric cooling over the SH in response to ozone depletion with cooling exceeding -2K, while tropospheric signals are largely insignificant. CO2 is also consistent with expectations: The direct radiative forcing from the well-mixed GHGs causes a small warming of the troposphere and a cooling of approximately -1K in the stratosphere. It is notable that the tropospheric warming due to GHG in the absence of indirect effects is fairly subtle. This limited warming occurs because all boundary conditions are held fixed and feedback mechanisms, which are responsible for most of the tropospheric warming associated with global warming, do not have an effect. In the SST experiment, the most pronounced changes take place. The increase in SSTs produces a tropospheric warming of at least 0.5K, with increases in excess of 1K occurring in the tropical upper troposphere and near the surface at northern high latitudes. This is consistent with our expectations that the troposphere has warmed by approximately 1K over the past century. The ALL experiment presents two prominent features: stratospheric cooling at southern high latitudes and significant tropospheric warming, which is maximized over the southern mid-latitudes. Comparing these findings with temperature trends seen in the ERA, there is overall consistency with only a few discrepancies, which are in most cases statistically insignificant. One particularly noteworthy aspect is the similarity between ALL and ERA. This good agreement between the observed trends and the model-simulated changes underscores the fact that much of the warming observed over the past century has in fact occurred since 1979.

The second column of Figure 2 depicts changes in the zonal wind (U). The most noticeable feature seen in O3 is a dipole structure in the vicinity of the SH jet, which represents a poleward shift of this feature as well as a possible increase in the altitude of

the jet core. The wind changes associated with this dipole extend all the way to the surface, although with somewhat reduced magnitude. CO2 produces weaker wind changes than O3, although we do again observe the aforementioned dipole structure. The exact mechanisms for these changes in wind are not well understood and are the subject of intense research (e.g., Chen and Held 2007). In accordance with previous findings (e.g., Thompson and Solomon 2002, Gillett and Thompson 2003), it is reasonable to assume that the stratospheric cooling evident in O3 and CO2 is at least partially responsible for the wind shift in the upper troposphere – lower stratosphere (UTLS) region, and that baroclinic interactions may play a role in extending it towards the surface. The SH dipole centered near the jet is developed even more strongly in the SST experiment, while a large increase (> 1 m/s), without a shift, in the NH jet is also noted. ALL maintains the same pattern as the SST experiment and reveals the most pronounced changes in U. The dipole over the SH is particularly well developed, with changes in wind ranging from -1 to +4 m/s. Comparing to the ERA40 reanalysis, remarkable similarity is again depicted and the existence of the SH dipole is confirmed. As indicated by the absence of hatching in ERA, the large increases in U located at 60S are significant throughout the troposphere and lower stratosphere.

In the third column of Figure 2 examine shifts in the meridional mass circulation (MMC), as it provides insights to changes in the strength and location of the primary atmospheric circulation cells. The climatology (black lines) clearly shows a strong Hadley cell over the winter hemisphere (NH), a weaker summer Hadley cell in the SH, the Ferrel cells, and the amorphous Polar cells. As before, the structure of the changes in all of the experiments exhibit a considerable degree of similarity, especially over the SH.

Noteworthy trends in O3 are restricted to the SH, where a poleward shift in the Ferrel cell and a poleward expansion of the Hadley cell are indicated. The other three experiments also produce these trends, with the SST experiment and ALL amplifying their magnitude. In addition, these experiments appear to shift the ITCZ southward and develop a stronger Ferrel cell over the NH. Confidence in reanalysis-derived changes in the MMC is low because they are dependent upon the meridional wind (V), which is a poorly observed quantity. Nevertheless, analyzing changes seen in ERA, the SH Hadley cell appears to be expanding poleward as the model predicted. Additionally, the northern Hadley cell becomes stronger.

The fourth column in Figure 2 displays the modeled and observed eddy momentum flux convergence, showing the meridional rearrangement of zonal momentum by eddies and the position of the eddy-driven jet (EDJ) – the clear maximum over each hemisphere depicted in the climatology. Both O3 and CO2 produce changes in momentum flux convergence that are dynamically consistent with the shifts in the position of the Ferrel cell seen in the results for the MMC. In particular, they develop a dipole centered on the southern hemisphere EDJ, indicating a poleward shift in this feature. Increased SSTs produce a strong response in both hemispheres, with strong dipoles noted in each. The shift in maximum flux convergence seen over the NH is less well developed than that over its SH counterpart. A number of interesting comparisons and contrasts are found in the observations, but the only large area of robust change occurs in the vicinity of the SH maximum, comparing very favorably with the model-derived changes.

The final column in Figure 2 shows changes in the location of the tropopause. All of our experiments depict similar alterations to the shape of the tropopause. These are characterized by both a rise in tropopause height and a poleward shift in the region of the tropical-extratropical transition, especially over the SH. Based on our experiments, changes in ozone and SSTs are primarily responsible for these shifts and they are clearly least developed in CO2. Changes in GHG concentrations do, however, seem to play a significant role in altering the tropopause structure over the NH, while changes in O_3 are more dominant over the SH. The observations in ERA show very similar changes to those in our experiments, as well as those described in Lu et al. (2009), but are also suggestive that high-latitude rises in tropopause altitude are slightly underestimated in the model simulations.

Summarizing, most circulation features exhibit strong poleward shifts in response to the imposed forcing, which are more pronounced over the SH. These shifts are statistically robust, and supported in most cases by the ERA40 reanalysis.

3.2 Change in Dynamical Circulation Indicators

Figure 3 shows the change in the latitudinal position of selected dynamical circulation indicators as a function of season. A complete list of these indicators and atmospheric features associated with them can be found in Table 2. For example, we explore two measures of zonal wind at the surface: the position of the zero-crossing between tropical easterlies and extratropical westerlies ($U_{SFC\text{-}ZC}$), and also that of the maximum westerlies ($U_{SFC\text{-}MAX}$). The position of maximum westerlies at 200 hPa ($U_{200\text{-}MAX}$) is also examined, along with the dynamically related location of maximum eddy

flux convergence, $-\partial/\partial y(\overline{u'v'})$. Two measures of the MMC are investigated: the boundary between the Hadley and Ferrel cells (Ψ_{EQTR}) and the boundary between the Ferrel and Polar cells (Ψ_{POLE}). Another feature of interest is the latitudinal position at which the tropopause occurs at a pressure 25 hPa below the tropical tropopause pressure (TROPO). Finally, we also analyze shifts in the AMs.

It is immediately apparent in Figure 3 that all indicators share a common seasonality and relatively similar magnitudes. For most measures, changes are fairly weak during the winter months for each respective hemisphere. This is in contrast to the rather robust shifts which occur during the summer months, consistent with the findings of Hu and Fu (2007). There are few exceptions to this generalization of the seasonal cycle – one notable example is seen in the NAM, for which we find two maxima occurring during the transitional seasons. Similarly, the SAM deviates from this pattern slightly in that shifts in this measure are weakest right before they become strongest, following the breakdown of the stratospheric vortex around October-November.

Nearly all indicators, during all seasons, are characterized by poleward shifts. These typically are on the order of 1-2° latitude, following the seasonal pattern described above. However, cases exist for which these poleward displacements approach 2.5° over the SH (TROPO, Ψ_{POLE}), and also for which even slight contractions occur over the NH (Ψ_{EQTR}, Ψ_{POLE}). This indicates that changes in the MMC, particularly in the Hadley circulation, may be difficult to predict. This is supported by the range of results obtained in prior studies (Hu and Fu 2007, Johanson and Fu 2009, Hu and Zhou 2010). To the best of our knowledge, the large seasonal variations in changes of the Ferrel cell have not been previously documented. We do find that the poleward expansion of the Hadley cell

Fig. 3 Change in the latitudinal position of dynamical circulation indicators for each experiment and the linear addition of O3, CO2, and SST (legend at bottom). The top (bottom) half of each panel shows results for the NH (SH). Numbers shown in the top and bottom right corner of each panel represent the mean annual position of a given indicator in degrees latitude derived from the control run (except for $U_{200\text{-}MAX}$, see text). Vertical bars show the length of the 95% confidence interval according to a two-sided T-test. Units on the Y-axis are in degrees latitude, except for the AM. X-axis shows the center month of a three month seasonal average. Note that January and February are each shown twice for clarity.

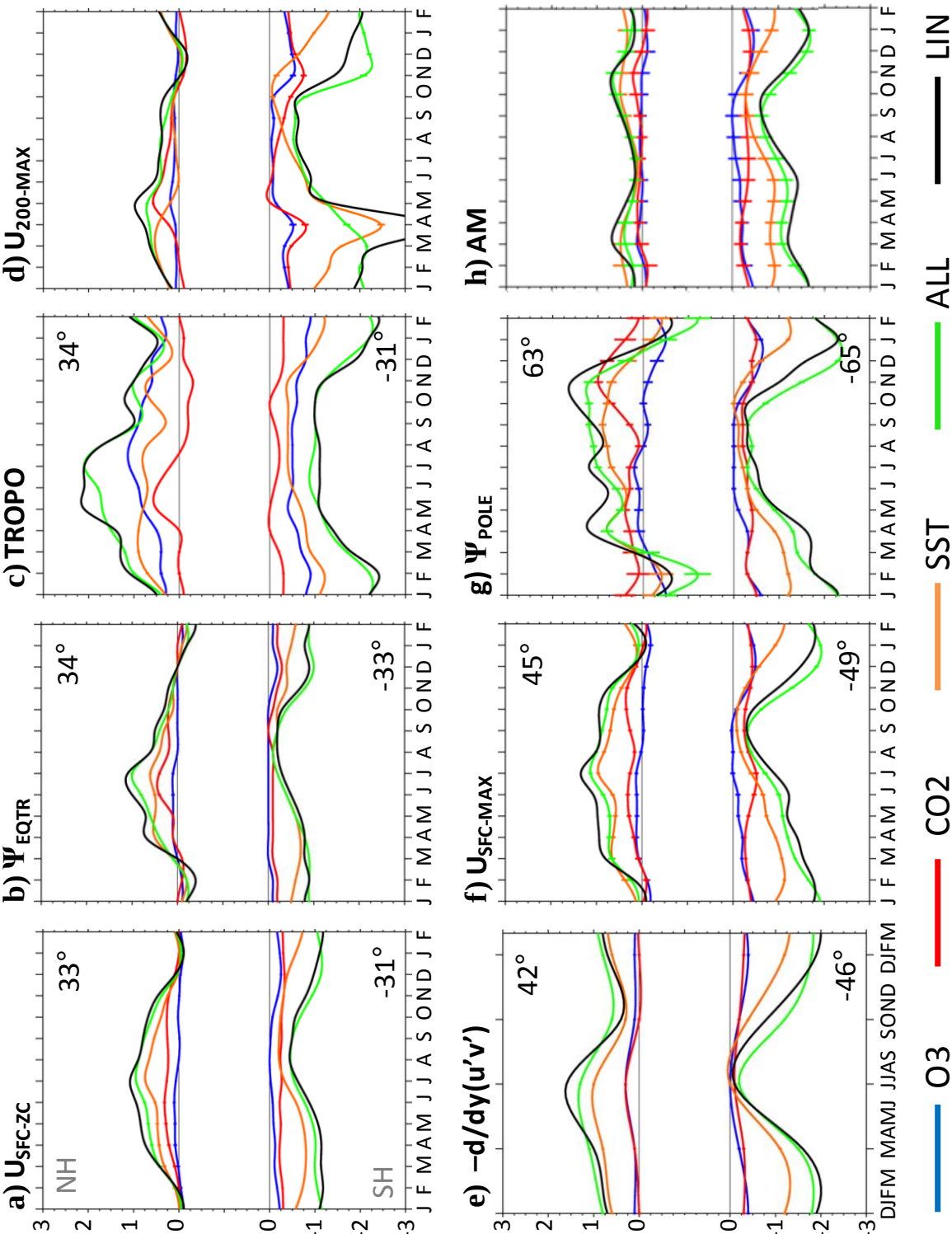
a) U SFC-ZC
b) Ψ EQTR
c) TROPO
d) U 200-MAX
e) −d/dy(u'v')
f) U SFC-MAX
g) Ψ POLE
h) AM
NH
SH
33°
-31°
34°
-33°
34°
-31°
42°
-46°
45°
-49°
63°
-65°
J F M A M J J A S O N D J F
DJFM MAMJ JJAS SOND DJFM
O3
CO2
SST
ALL
LIN

Table 2 Overview of symbols and circulation indicators.

Symbol	Description	Atmospheric Feature	Units
[ ]	zonal-mean		
T	temperature		K
U	zonal wind		m/s
Ψ	meridional mass streamfunction (MMC)		kg/s
$-\delta/\delta y(u'v')$	eddy momentum flux convergence		m/s^2
TROPO	probability distribution function of tropopause occurrences		days/season
P-E	precipitation minus evaporation		$kg/(m^2*s)$
U_{SFC_ZC}	zero-crossing of U at the surface	poleward edge of Hadley cell	lat
Ψ_{EQTR}	equatorward zero-crossing of Ψ	poleward edge of Hadley cell	lat
TROPO	tropopause location 25 hPa below the tropical tropopause	poleward edge of Hadley cell	lat
$U_{SFC\text{-}MAX}$	maximum of U at the surface	eddy-driven jet, storm track	lat
$-\delta/\delta y(u'v')_{MAX}$	maximum of eddy momentum flux convergence	eddy-driven jet, storm track	lat
$U_{200\text{-}MAX}$	maximum of u at 200 hPa	jet	lat
Ψ_{POLE}	poleward zero-crossing of Ψ	poleward edge of Ferrel cell	lat
AM	annular modes calculated from sea level pressure from 20S-90S and 20N-90N		index
ITCZ	global precipitation maximum	intertropical convergence zone	lat
$P\text{-}E_{EQTR}$	equatorward zero-crossing of P-E	boundary of inner/outer tropics	lat
$P\text{-}E_{MIN}$	hemispheric minimum of in P-E	subtropics	lat
P_{MIN}	hemispheric minimum in precipitation	subtropics	lat
$P\text{-}E_{POLE}$	poleward zero-crossing of P-E	boundary of sub/extra tropics	lat
P_{MAX}	hemispheric maximum in precipitation	storm track	lat
$P\text{-}E_{MAX}$	hemispheric maximum in P-E	extratropics	lat

and EDJ does roughly follow the 1:2 relationship put forth by Kang and Polvani (2010). Increases in the AMs are also consistent with the poleward shifts of other indicators.

The statistical significance of our results is found to be very high. The significance of shifts seen in indicators further from the equator tends to be slightly lower, likely to some degree a product of the higher variability at these latitudes. Only for Ψ_{POLE} and the AMs are there certain seasons for which doubt is cast on the sign of the changes.

There are a number of relationships apparent in Figure 3. An excellent comparison can be made between Ψ_{EQTR}, and $U_{SFC\text{-}ZC}$, which should coincide directly with the downwelling branch of the Hadley circulation and the position of the subtropical highs at the surface. There is also good agreement between the changes seen in $-\partial / \partial y$ (u'v'), $U_{SFC\text{-}MAX}$, and Ψ_{POLE}. This agreement is to be expected given the linkages between eddy momentum flux convergence, the EDJ, and the location of the Ferrel cell. For both these sets of similar features, the agreement tends to be even more evident over the SH, although it is good over the NH as well.

We observe that over the SH, changes in $U_{MAX\text{-}200}$ undergo pronounced "jumps" during the transitional seasons. During these times, a dual jet regime tends to develop over the SH. Because of the difficulty in differentiating between the STJ and EDJ, we actually alternate between measuring the STJ during the cool season (May-October) and a combination of the STJ and EDJ during the warm season (November-April). Thus, the "jumps" seen in our analysis of changes in $U_{MAX\text{-}200}$ occur because shifts of the EDJ are rather large (2° latitude), while those for the STJ are much smaller (1° latitude). The particularly odd behavior of changes in $U_{MAX\text{-}200}$ seen during MAM over the SH is due to

slight changes in the structure of the "broad" climatological maximum of this feature. Once again, we find support for the 1:2 ratio suggested by Kang and Polvani (2010). Because of the meridional gradient in temperature that exists at the transition from the tropical to extratropical tropopause, TROPO is dynamically coupled to $U_{200\text{-}MAX}$ via the thermal wind relationship. We note that although similar, the seasonal transitions noted in TROPO are not as pronounced. However, due to the dynamical linkage, the analysis of TROPO may suffer from similar difficulties.

Examining the model-produced shifts for each of our experiments, it is clear that the indirect contribution associated with SST changes is dominant. TROPO, however, is also significantly affected by ozone forcing (Son et al. 2009b). The forcing from O_3 losses over the SH exhibits a clear seasonal signature (see Figure 1), coinciding with a similar seasonal structure in circulation indicators (blue). This is seen most clearly in high latitude features such as Ψ_{POLE}, and the SAM. The signal becomes strongly evident around November (coinciding with the breakdown of the stratospheric vortex), before waning through austral summer and spring. For most measures, the individual contribution from changes in GHG concentrations is nearly invariant, changing little from one month to the next.

Interestingly, there is remarkable agreement between the magnitude and seasonality of shifts produced by ALL and those obtained from a linear addition (LIN) of the other three experiments. This reinforces the findings of Fomichev et al. (2007) and Deser and Phillips (2009) – that individual atmospheric forcings are approximately additive.

3.3 Change in Hydrological Circulation Indicators

Along with dynamical measures, we also investigate a number of hydrological indicators. Figure 4 roughly shows the meridional profiles of precipitation (top) and precipitation minus evaporation, or P-E (bottom), indicating approximately where our hydrological indicators are located. As with the dynamical indicators, a complete list of these can be found in Table 2. We examine three indicators that are based solely on precipitation (Figure 4, top): the position of the Inter-tropical convergence zone (ITCZ), and also the locations of the subtropical minimum (P_{MIN}) and extratropical maximum (P_{MAX}) in precipitation for each respective hemisphere. In addition, we analyze measures of precipitation minus evaporation (Figure 4, bottom): the hemispheric minimum (P-E_{MIN}) and maximum (P-E_{MAX}) in P-E, and the boundaries where P-E is 0, which occur at the transitions between the inner and outer tropics (P-E_{EQTR}), and also between the subtropics and extratropics (P-E_{POLE}). Figure 5 presents the seasonal change in the latitudinal position of these features.

Figure 5 shows a high degree of agreement between most hydrological indicators, although there exists slightly more variation than seen in the dynamical ones. Of greatest interest is the similarity in the sign of shifts, as nearly all measures are found to be displaced poleward, with few exceptions. P-E_{EQTR} exhibits an equatorward shift over the NH, which we suggest is in fact consistent with the possibility of contraction seen in Ψ_{EQTR} over the NH during boreal winter, since both are products of the Hadley circulation. The other southward-displaced indicator is the ITCZ, which is consistent with changes in P-E_{EQTR} as it aligns more closely to the equator. Examining further, the three indicators closest to the equator (ITCZ, P-E_{EQTR}, P-E_{MIN}) exhibit shifts that are

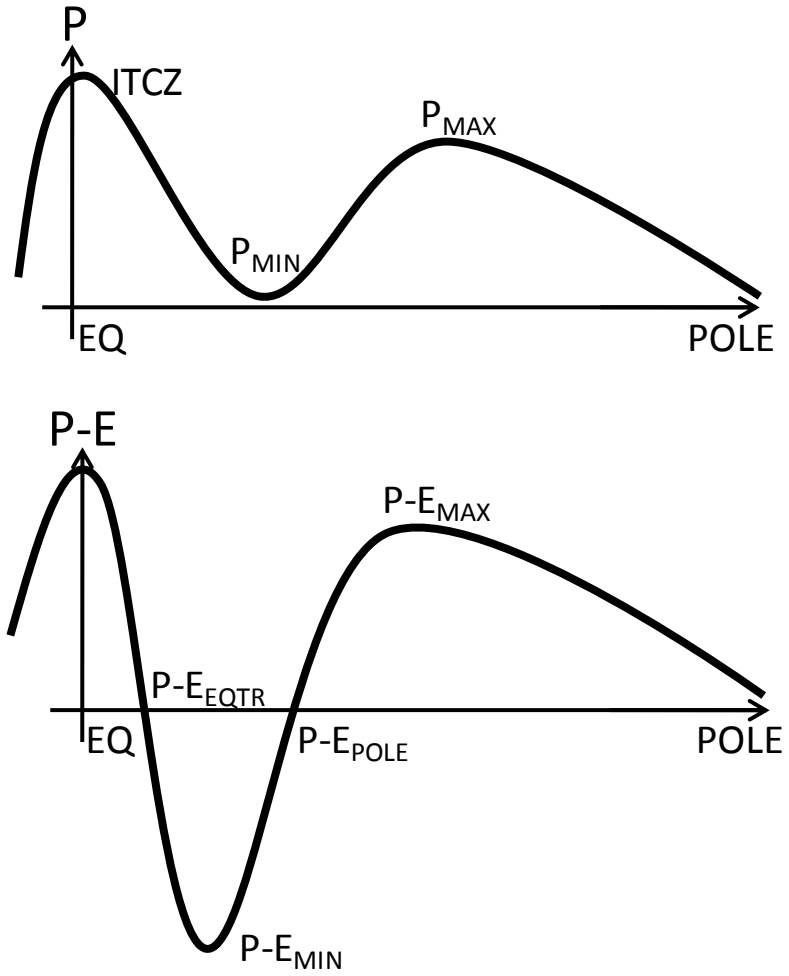

Fig. 4 Schematic showing the location of moisture-based measures: Precipitation (top) and P-E (bottom).

Fig. 5 As Fig. 3, except for hydrological indicators. The Y-axis for the ITCZ is centered on zero (e.g. our results indicate a 0-1° southward shift of this feature).

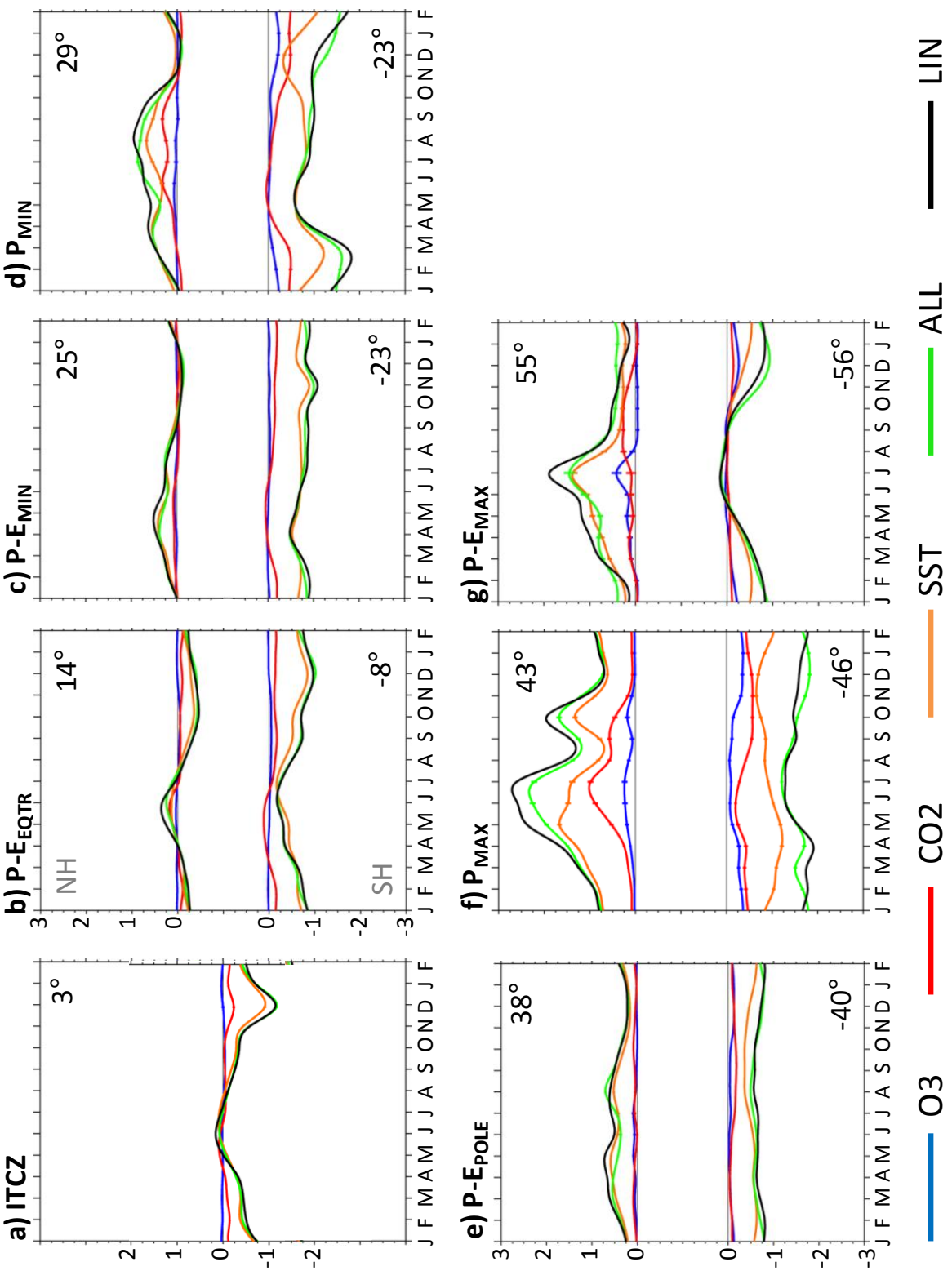
a) ITCZ
b) P-E_EQTR
c) P-E_MIN
d) P_MIN
e) P-E_POLE
f) P_MAX
g) P-E_MAX
NH
SH
3°
14°
25°
29°
38°
43°
55°
-8°
-23°
-40°
-46°
-56°
J F M A M J J A S O N D J F
O3
CO2
SST
ALL
LIN

dynamically consistent with a southward shift of the zone of the inner tropics, anchored on the ITCZ. This is apparent noting that shifts over the NH for these features ($P\text{-}E_{EQTR}$ and $P\text{-}E_{MIN}$) are minimal, while those over the SH are more clearly poleward, an aspect that we do not believe has been previously mentioned. Examining P_{MIN}, this result can also be inferred to hold true, to some extent, at the edge of the Hadley cells.

There seem to be two primary "modes" of model-produced shifts seen in hydrological indicators. The first consists of moderate poleward shifts in location of about 1° latitude that are relatively uniform throughout the seasonal cycle. The second is characterized by strong seasonality – amplitudes approaching 2° latitude – especially over the NH, with the most significant changes occurring during the summer months of each respective hemisphere. These findings are largely consistent with the changes we see in dynamical indicators. It is interesting that these modes are favored by features closer to the equator (ITCZ, $P\text{-}E_{EQTR}$, $P\text{-}E_{MIN}$, $P\text{-}E_{POLE}$) and closer to the poles (P_{MAX}, $P\text{-}E_{MAX}$), respectively. Changes in P_{MIN} exhibit a behavior that is somewhere between these two extremes. This may be partially explained by noting that measures of changes in P are more seasonally variable than those for measures of P-E, which are smoother. Additionally, changes in the minima and zero-crossings of these measures are more seasonally uniform than those for the maxima.

The sign and magnitude of shifts seen in P_{MAX} and $P\text{-}E_{MAX}$ are well correlated with those seen in several dynamical indicators: $-\partial/\partial y(\overline{u'v'})$, $U_{SFC\text{-}MAX}$, and Ψ_{POLE}. All these features are related to the location of the EDJ and the concomitant storm tracks. Although first order consistency exists, there is also an interesting disagreement between the hydrological and dynamical measures. While the hydrological indicators are most

strongly displaced over the NH during boreal summer, the dynamical indicators are significantly shifted during summer over both hemispheres, perhaps more strongly (> 2° latitude) over the SH. Despite these dynamical shifts, changes in P_{MAX} and $P\text{-}E_{MAX}$ exhibit a relatively smooth annual structure. In other words, although shifts in the large-scale dynamics of the circulation over the SH undergo a significant seasonal cycle, the shifts in hydrological features do not. Furthermore, there is an indication that, over the SH, this is more true for precipitation than for P-E, which does show some seasonality.

The results from our experiments show that, as for dynamical indicators, SST is again the dominant contributor to modeled shifts. In fact, it could be argued that SST alterations are even more crucial for the shifts of these hydrological indicators than seen previously for those based on dynamics. We believe this may be linked to the strong coupling of the oceans and atmosphere in the hydrological cycle. Contributions from ozone depletion and increased GHGs play a very small role for all hydrological indicators and seasons, although ozone changes do affect changes in the location of the precipitation minimum and maximum over the SH. Only for P_{MIN} does the contribution from one of these forcings (GHGs) ever supersede that from changes in SST. As shown previously, there is once again exceptional agreement between the changes in ALL and changes obtained from a linear addition (LIN) of those from the other three experiments. We again note that this result remains valid throughout the seasonal cycle.

As with the dynamical indicators, we find the statistical significance of these results to be very high. Only at high latitudes do we start to see the slightest uncertainty.

So far, we have purposefully considered only the zonal-mean profiles of basic atmospheric quantities and selected circulation indicators in our analysis. We

acknowledge that this is a gross over-simplification of the spatial patterns observed in the atmosphere. To highlight this point, we present the model-produced annual changes in P-E in Figure 6, highlighting the global distribution of shifts in this field, which forms the basis of many of our hydrological indicators. This figure provides a fuller sense of the differences between regional and zonal-mean shifts in hydroclimate and of the complexity of attempting to resolve the roles of anthropogenic forcings.

Specifically, note the contrasting influences of increases in GHG concentrations and changes in SST on areas near the Sahel region of western Africa, both of which produce significant results. The ALL experiment confirms the canceling effects of these individual forcings, but there are questions as to how reliable these model-produced results may be. Accurately predicting these changes is of particular importance in regions such as the Sahel, where changing hydroclimate has already placed huge strains on the inhabitants.

When considering the zonal-mean profiles to the right in Figure 6, it is seen that shifts in P-E are quite small in the CO2 experiment, corresponding well with the previous examination of our indicators. The SST experiment, however, produces significant shifts in P-E, which are largely reproduced with only minor differences in the ALL experiment. In describing these shifts, it is useful to say that in general the wet regions become wetter, while the dry regions become drier. More specifically, moistening occurs in the tropical latitudes around the equator and in the extratropics, while subtropical regions experience drying.

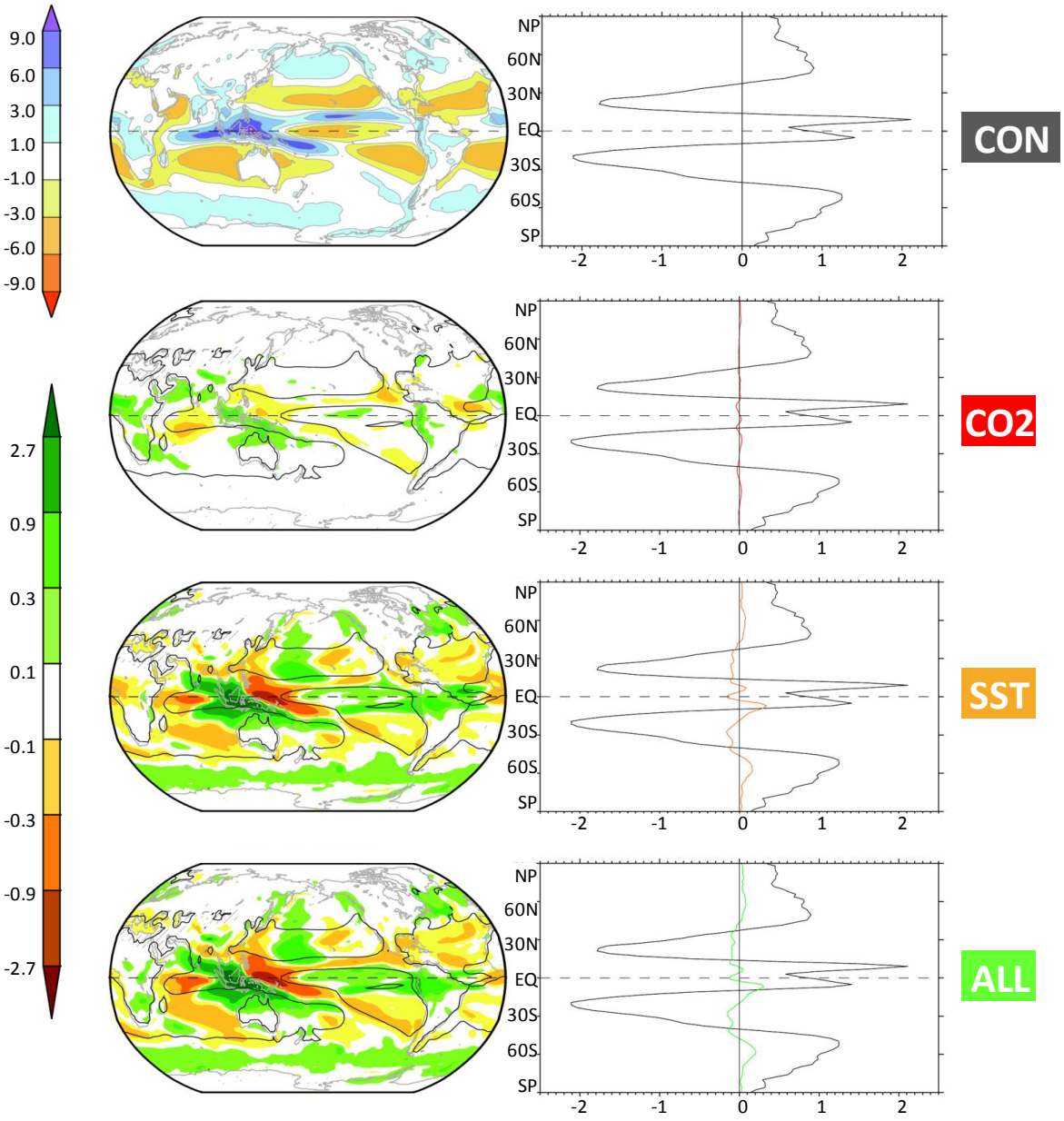

Fig. 6 Spatial distribution of annual mean change in P-E. Units for all scales are mm/day. The thin black line denotes where P-E = 0 (left column) and zonal-mean P-E (right column) derived from the control run. The top row depicts the climatological annual P-E for the full field (left) and in the zonal-mean (right). For each of our experiments (except O3 – not shown because only minor shifts occur), shading on the left denotes spatial change in P-E, while the colored lines on the right show change in zonal-mean P-E. Hatching shows changes which are nonsignificant according to a two-sided T-test at the 95% confidence interval.

CHAPTER 4

SUMMARY AND DISCUSSION

Long simulations performed using the GFDL AM2.1 are used to diagnose anthropogenically-induced shifts in the general circulation since the pre-industrial era. Our results are to a large extent consistent with both the ERA40 reanalysis and the findings of previous studies. Summarizing, we find that changes in the atmospheric circulation have been characterized by clear poleward trends in many important indicators, consistent with an increase of the AMs (see Figure 7). These trends are on the order of 0.5 to 1.5° latitude in the annual mean and exceed 2° latitude for some features during favored seasons. These results are valid not only for previously investigated indicators, but newly explored features as well. Along with these poleward shifts, an increase in the altitude of some features, such as the tropopause and the jet, is also noted. Indirect forcing (represented by our SST experiment) is primarily responsible for nearly all of these shifts, but GHG increases and ozone depletion, especially over the SH, also play important roles. Additionally, the effects of individual forcings on the circulation are nearly additive – in agreement with Deser and Phillips (2009).

An investigation of the seasonality associated with changes in major atmospheric features is an important aspect of this study. With the exception of some P-E features, changes in most circulation indicators over the SH exhibit a stronger magnitude and

Fig. 7 Mean annual change of circulation indicators. Results for our four experiments, as well a linear addition of O3, CO2, and SST are presented. Colors follow the scale at right.

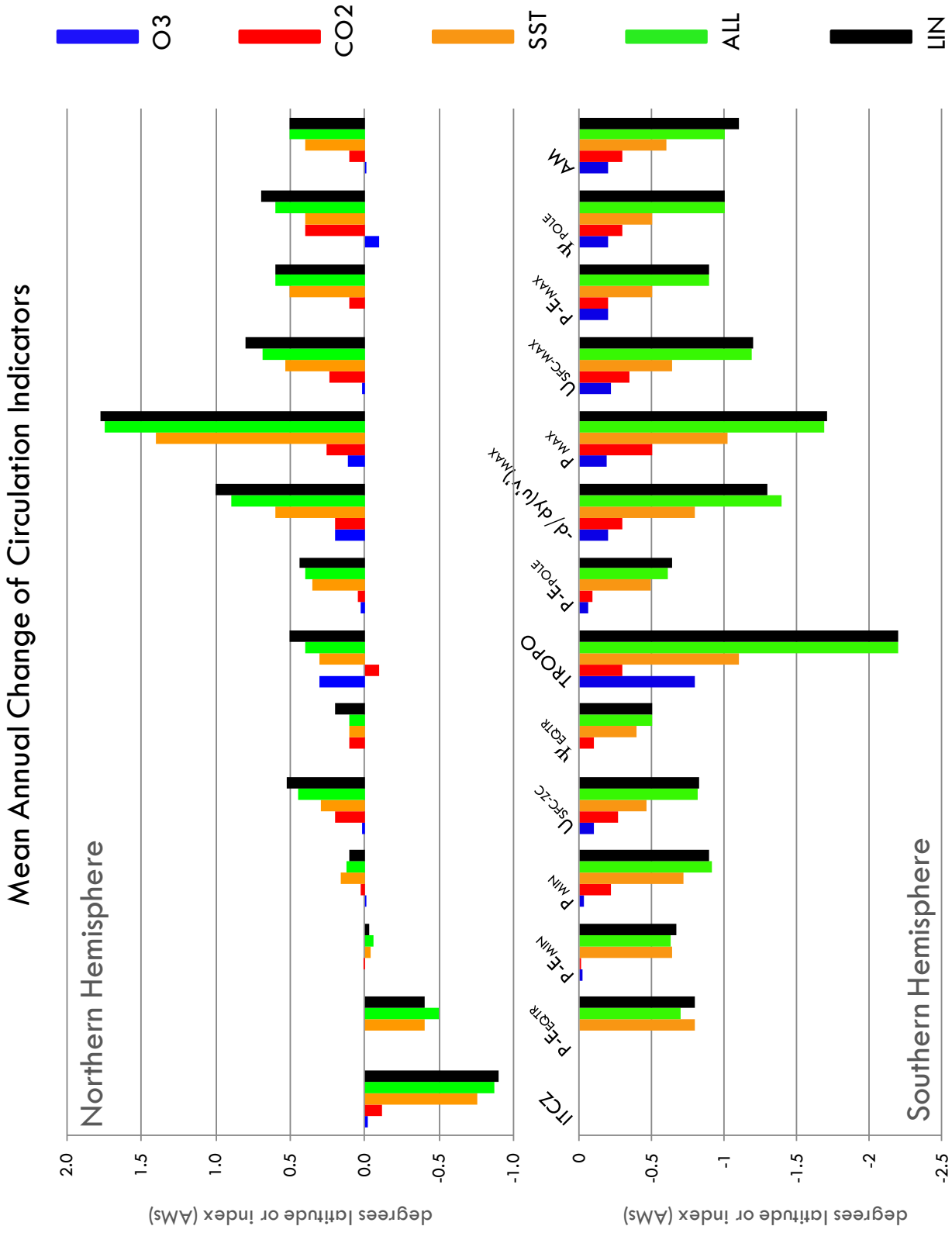
Mean Annual Change of Circulation Indicators
O3
CO2
SST
ALL
LIN
Northern Hemisphere
Southern Hemisphere
degrees latitude or index (AMs)
2.0
1.5
1.0
0.5
0.0
-0.5
-1.0
0
-0.5
-1
-1.5
-2
-2.5
ITCZ
P-EEQTR
P-EMIN
PMIN
USFC-ZC
YEQTR
TROPO
P-EPOLE
-d/dy(u'v')MAX
PMAX
USFC-MAX
P-EMAX
YPOLE
AM

seasonality as compared to those over the NH, contrasting with the results from the observational study by Hu and Fu (2007) in which both hemispheres exhibited more equal shifts. These changes are also more pronounced and more seasonally variable as one moves poleward, suggestive of a greater impact at high latitudes. We find evidence for an overall southward shift of the inner tropics, as well as an expansion of the Hadley circulation and subtropical dry zones. Consistent with this widening of the entire tropical belt is a poleward shift of the Ferrel cell and its associated features: the EDJ and storm tracks being the most prominent.

There are also a number of caveats to this study, which deserve further discussion. Our study is performed using primarily zonal-mean data, which provides a number of advantages; most notably a reduction in complexity. However, this can be misleading without caution taken to realize that in the full field, many variables of climate interest are spatially very inhomogeneous and exhibit complicated patterns that are difficult to understand. We also take 3-month running averages. The advantage of this approach is that our analysis produces more gradual seasonal transitions. Similarly to our use of zonal-mean data, the drawback is once again that these averages can blur the magnitude of atmospheric phenomena occurring or being maximized on smaller scales, in this case – shorter time scales. Finally, our results are based on the outcomes of only one model.

REFERENCES

Arblaster, J.M. and G.A. Meehl, 2006: Contributions of External Forcings to Southern Annular Mode Trends. *J. Climate*, **19**, 2896–2905, doi: 10.1175/JCLI3774.1

Archer, C.L. and K. Caldeira 2008: Historical Trends in the Jet Streams. *Geophys. Res. Lett.*, **35**, L08803

Baldwin M.P. and T.J. Dunkerton, 2001: Stratospheric Harbingers of Anomalous Weather Regimes. *Science*, **294**, (5542): 581-584

Baldwin, M.P., and D.W.J. Thompson, 2009: A Critical Comparison of Stratosphere-Troposphere Coupling Indices. *Q. J. R. Meteorol. Soc.*, final version; 1661-1672.

Battisti, D.S. and R.L. Naylor, 2009: Historical Warnings of Future Food Insecurity with Unprecedented Seasonal Heat. *Science*, **323**, (5911): 240-244

Bengtsson, L., Hodges, K.I., and E. Roeckner, 2006: Storm Tracks and Climate Change. *J. Climate*, **19**, 3518–3543.

Bengtsson, L., Hodges, K.I., and N. Keenlyside, 2009: Will Extratropical Storms Intensify in a Warmer Climate? *J. Climate*, **22**, 2276–2301.

Butler, A.H., Thompson, D.W.J., and R. Heikes, 2009: The Steady-State Atmospheric Circulation Response to Climate Change-Like Thermal Forcings in a Simple Circulation Model. *J. Climate* (submitted and accepted, 2009).

Chen, W.-T., Liao, H., and J. Seinfeld, 2007: Future Climate Impacts of Direct Radiative Forcing of Anthropogenic Aerosols, Tropospheric Ozone, and Long-lived Greenhouse Gases. *J. Geophys. Res.*, **112**, D14209

Chen, G. and I.M. Held, 2007: Phase Speed Spectra and the Recent Poleward Shift of Southern Hemisphere Surface Westerlies. *Geophys. Res. Lett.*, **34**, L21805

Cohen, J. and M. Barlow, 2005: The NAO, the AO, and Global Warming: How Closely Related? *J. Climate*, **18**, 4498–4513.

Deser, C. and A.S. Phillips, 2009: Atmospheric Circulation Trends, 1950–2000: The Relative Roles of Sea Surface Temperature Forcing and Direct Atmospheric Radiative Forcing. *J. Climate*, **22**, 396–413, doi: 10.1175/2008JCLI2453.1

Fomichev, V.I., Jonsson, A.I., de Grandpré, J., Beagley, S.R., McLandress, C., Semeniuk, K., and T.G. Shepherd, 2007: Response of the Middle Atmosphere to CO2 Doubling: Results from the Canadian Middle Atmosphere Model. *J. Climate*, **20**, 1121–1144,
doi: 10.1175/JCLI4030.1

Gastineau, G., Laurent, L., and H. Le Treut, 2009: The Hadley and Walker Circulation Changes in Global Warming Conditions Described by Idealized Atmospheric Simulations. *J. Climate*, **22**, 3993–4013, doi: 10.1175/2009JCLI2794.1

Gillett, N.P. and D.W.J. Thompson, 2003: Simulation of Recent Southern Hemisphere climate change. *Science*, **302**, 273-275

Gillett, N.P., Zwiers, F.W., Weaver, A.J., and P.A. Stott, 2003: Detection of Human Influence on Sea-level Pressure. *Nature*, **422**, 292-294.

Gillett, N.P., Allan, R.J., and T.J. Ansell, 2005: Detection of External Influence on Sea-level Pressure with a Multi-model Ensemble. *Geophys. Res. Lett.*, **32**

Gillett, N.P., Kell, T.D., and P.D. Jones, 2006: Regional Climate Impacts of the Southern Annular Mode. *Geophys. Res. Lett*,. **33**

Gillett, N.P., and P.A. Stott, 2009: Attribution of Anthropogenic Influence on Seasonal Sea-level Pressure. *Geophys. Res. Lett.*, **36**

Hu, Y. and Q. Fu, 2007: Observed Poleward Expansion of the Hadley Circulation since 1979. *Atmos. Chem. Phys.*, **7,** 5229-5236

Hu, Y., and C. Zhou, 2010: Observational Evidence for the Poleward Expansion of the Hadley Circulation. *Adv. Atmos. Sci.,* doi: 10.1007/s00376-010-0032-1.

Johanson, C.M. and Q. Fu: Hadley Cell Expansion: Model Simulations Versus Observations. *J Climate* (submitted, 2009).

Kang, S.M. and L.M. Polvani: The Interannual Relationship Between the Eddy-driven Jet and the Edge of the Hadley Cell in Austral Summer, *J. Climate* (submitted, 2010).

Karoly, D.J., 2003: Ozone and Climate Change. *Science*, **302**, (5643): 236-237

Karpechko, A.Y., Gillett, N.P., Marshall, G.J., and A.A. Scaife, 2008: Stratospheric Influence on Circulation Changes in the Southern Hemisphere Troposphere in Coupled Climate Models. *Geophys. Res. Lett.*, **35**.

Kushner, P.J., Held, I.M., and T.L. Delworth, 2001: Southern-hemisphere Atmospheric Circulation Response to Global Warming. *J. Climate*, **14**, 2238-2249.

Kuzmina, S., Bengtsson, L., Johannessen, O.M., Drange, H., Bobylev, L.P., and M.W. Miles, 2005: The North Atlantic Oscillation and Greenhouse-gas Forcing. *Geophys. Res. Lett.,* **32**, doi:10.1029/2004GL021064

Lin, S.-J., 2004: A "Vertically Lagrangian" Finite-Volume Dynamical Core for Global Models. *Mon. Wea. Rev.*, **132,** 2293-2307.

Lorenz, D.J. and E.T. DeWeaver, 2007: Tropopause Height and Zonal Wind Response to Global Warming in the IPCC Scenario Integrations. *J. Geophys. Res.,* **112** (D10119), doi:10110.11029/12006JD008087

Lu, J., Vecchi, G.A., and T. Reichler, 2007: Expansion of the Hadley Cell under Global Warming. *Geophys. Res. Lett.,* **34**, doi: 10.1029/ 2006GL028443

Lu, J., Deser, C., and T. Reichler, 2009: Cause of the Widening of the Tropical Belt since 1958. *Geophys. Res. Lett.,* **36,** (L03803), doi: 10.1029/2008GL036076

Miller, R.L., Schmidt, G.A., and D.T. Shindell, 2006: Forced Annular Variations in the 20th Century Intergovernmental Panel on Climate Change Fourth Assessment Report Models. *J. Geophys. Res.,* **111**, (D18101), doi:10.1029/2005JD006323

Mitas, C.M. and A. Clement, 2005: Has the Hadley Cell been Strengthening in Recent Decades? *Geophys. Res. Lett*., **32**, doi: 10.1029/ 2004GL021765

Mitas, C.M. and A. Clement, 2006: Recent Behavior of the Hadley Cell and Tropical Thermodynamics in Climate Models and Reanalyses. *Geophys. Res. Lett.,* **33**, (L01810), doi: 10.1029/ 2005GL024406

Moritz, R.E., Bitz, C.M., and E.J. Steig, 2002: Dynamics of Recent Climate Change in the Arctic. *Science,* **297** (5586), 1497.

Overland, J.E. and M. Wang, 2005: The Arctic Climate Paradox: The Recent Decrease of the Arctic Oscillation. *Geophys. Res. Lett.*, **32**, (L06701).

Perlwitz, J., Pawson, S., Fogt, R.L., Nielsen, J.E., and W.D. Neff, 2008: Impact of Stratospheric Ozone Hole Recovery on Antarctic Climate. *Geophys. Res. Lett.*, **35**, (L08714), doi:10.1029/2008GL033317

Previdi, M., and B.G. Liepert, 2007: Annular Modes and Hadley Cell Expansion under Global Warming. *Geophys. Res. Lett.*, **34**, (L22701), doi: 10.1029/2007GL031243

Randel, W.J., Wu, F., and D.J. Gaffen, 2000: Interannual Variability of the Tropical Tropopause Derived from Radiosonde Data and NCEP Reanalyses, *J. Geophys. Res.*, **105,** 15,509-15,523.

Randel, W.J., Wu, F., and R. Stolarski, 2002: Changes in Column Ozone Correlated with the Stratospheric EP Flux**.** *J. Meteorol. Soc. Japan,* **80**, 849-862.

Randel, W.J., Seidel, D.J., and L.L. Pan, 2007: Observational Characteristics of Double Tropopauses, *J. Geophys. Res.,* **112,** (D07309), doi: 10.1029/2006JD007904

Reichler, T. and J. Kim, 2008: How Well do Coupled Models Simulate Today's Climate? *Bull. Amer. Meteor. Soc.,* **89,** 303-311.

Reichler, T., Dameris, M., and R. Sausen, 2003: Determination of Tropopause Heights from Gridded Data. *Geophys. Res. Lett.,* **30**, No. 20, 2042, doi: 10.1029/2003GL018240.

Reichler, T., 2009: Changes in the Atmospheric Circulation as Indicator of Climate Change. in: *Climate Change: Observed Impacts on Planet Earth*, T. M. Letcher, Ed., Elsevier BV, The Netherlands, ISBN: 978-0-444-53301-2, pp. 145-164.

Santer, B.D., Wigley, T.M.L., Boyle, J.S., Gaffen, D.J., Hnilo, J.J., Nychka, D., Parker, D.E., and K. E. Taylor, 2000: Statistical Significance of Trends and Trend Differences in Layer-average Atmospheric Temperature Time Series. *J. Geophys. Res.*, **105,** 7337-7356

Santer, B. D., Sausen, R., Wigley, T.M.L., Boyle, J.S., AchutaRao, K., Doutriaux, C., Hanse, J.E., Meehl, G.A., Roeckner, E., Ruedy, R., Schmidt, G., and K.E. Taylor, 2003a: Behavior of Tropopause Height and Atmospheric Temperature in Models, Reanalyses, and Observations: Decadal Changes. *J. Geophys. Res.*, **108**, 4002.

Santer, B.D., Wehner, M.F., Wigley, T.M.L., Sausen, R., Meehl, G.A., Taylor, K.E., Ammann, C., Arblaster, J., Washington, W.M., Boyle, J.S., and W. Brüggemann, 2003b: Contributions of Anthropogenic and Natural Forcing to Recent Tropopause Height Changes. Science 301:479-483

Seager, R., Ting, M., Held, I., Kushnir, Y., Lu, J., Vecchi, G., Huang, H.-P., Harnik, N., Leetmaa, A., Lau, N.-C., Li, C., Velez, J., and N. Naik, 2007: Model Projections of an Imminent Transition to a More Arid Climate in Southwestern North America. *Science,* **316**, (5828): 1181-1184, doi:10.1126/science.1139601

Seidel, D.J. and W.J. Randel, 2007: Recent Widening of the Tropical Belt: Evidence from Tropopause Observations, *J. Geophys. Res.*, **112,** (D20113), doi: 10.1029/2007JD008861

Seidel, D.J., Fu, Q., Randel, W., and T. Reichler, 2008: Widening of the Tropical Belt in a Changing Climate, *Nature*, **Vol. 1, Jan. 2008**, doi: 10.1038/ngeo.2007.38

Son, S.-W. et al., 2008: The Impact of Stratospheric Ozone Recovery on the Southern Hemisphere Westerly Jet, *Science*, **320,** (5882)**:** 1486-1489, doi: 10.1126/science.1155939

Son, S., Tandon, N.F., Polvani, L.M., and D.W. Waugh, 2009a: The Ozone Hole and Southern Hemisphere Climate Change. *Nature* (submitted).

Son, S.-W., Polvani, L.M., Waugh, D.W., Birner, T., Akiyoshi, H., Garcia, R.R., Gettelman, A., Plummer, D.A., and E. Rozanov, 2009b: The Impact of Stratospheric Ozone Recovery on Tropopause Height Trends. *J. Climate,* **22**, 429-445.

Strong, C. and R.E. Davis, 2008: Variability in the Position and Strength of Winter Jet Stream Cores Related to Northern Hemisphere Teleconnections. *J. Climate*, **21**, 584-592.

Thompson, D.W.J. and S. Solomon, 2002: Interpretation of Recent Southern Hemisphere Climate Change, *Science*, **296**, (5569): 895-899, doi: 10.1126/science.1069270

Uppala, S.M. et al., 2005: The ERA-40 Re-analysis. *Quart. J. Roy. Meteor. Soc.*, **612**, (B):2961-3012(2952)

Wilks, D.S., 2006: *Statistical Methods in the Atmospheric Sciences*, 2nd edition (Elsevier)

Yin, J.H., 2005: A Consistent Poleward Shift of the Storm Tracks in Simulations of 21st Century Climate. *Geophys. Res. Lett.*, **32**, (L18701), doi:18710.11029/12005GL02368